

Received 16 August 2025, accepted 16 September 2025,
date of publication 23 September 2025, date of current version 30 September 2025.

Digital Object Identifier 10.1109/ACCESS.2025.3613598



RESEARCH ARTICLE

Subjective and Objective Quality Evaluation of Super-Resolution Enhanced Broadcast Images on a Novel SR-IQA Dataset

YONGROK KIM¹, JUNHA SHIN¹, JUHYUN LEE^{2,3}, AND HYUNSUK KO¹, (Member, IEEE)

¹Department of Electrical and Electronic Engineering, Hanyang University, Ansan 15588, South Korea

²Department of Bioengineering, The University of Texas at Arlington, Arlington, TX 76019, USA

³Department of Electrical Engineering and Computer Science, Daegu Gyeongbuk Institute of Science and Technology, Daegu 42988, South Korea

Corresponding author: Hyunsuk Ko (hyunsuk@hanyang.ac.kr)

This work was supported by the National Research Foundation of Korea (NRF) funded by Korean Government [Ministry of Science and ICT (MSIT)] under Grant RS-2023-00250751.

This work involved human subjects or animals in its research. Approval of all ethical and experimental procedures and protocols was granted by the Hanyang University Institutional Review Board under Application No. HYUIRB-202102-012.

ABSTRACT Super-Resolution (SR) is essential for displaying low-quality broadcast content on high-resolution screens. Recently, SR methods have been developed that not only increase resolution while preserving the original image information but also enhance the perceived quality. However, evaluating the quality of SR images generated from low-quality sources, such as SR-enhanced broadcast content, is challenging due to the need to consider both distortions and improvements. Additionally, assessing SR image quality without original high-quality sources presents another significant challenge. Unfortunately, there has been a dearth of research specifically addressing the Image Quality Assessment (IQA) of SR images under these conditions. In this work, we introduce a new IQA dataset for SR broadcast images in both 2K and 4K resolutions. We conducted a subjective quality evaluation to obtain Mean Opinion Score (MOS) for these SR images and performed a comprehensive human study to identify key factors influencing perceived quality. Finally, we evaluated the performance of existing IQA metrics on our dataset. This study reveals the limitations of current metrics, highlighting the need for a more robust IQA metric that better correlates with the perceived quality of SR images. The proposed dataset and the subjective evaluation platform are publicly available at <https://sites.google.com/hanyang.ac.kr/ivml/datasets/sreb>

INDEX TERMS Broadcast content, image quality assessment (IQA), IQA dataset, subjective image quality test, super-resolution.

I. INTRODUCTION

The demand for high-resolution content has escalated with advancements in various visual media services, including broadcasting, streaming services like YouTube, and Over-the-Top (OTT) platforms, driven by the ever-increasing resolution of display devices. Televisions, for instance, have transitioned from 2K to 4K resolution, and currently, there is a rapid proliferation of 8K TVs. In response to this evolving trend, content providers are not only producing new high-resolution

The associate editor coordinating the review of this manuscript and approving it for publication was Senthil Kumar .

content but also focusing on converting previously acquired low-resolution content to higher resolutions. In this context, Super-Resolution (SR) technology, which reconstructs High-Resolution (HR) images from Low-Resolution (LR) images, has emerged as a key area of research. With the advancements in deep learning, various deep learning-based SR methods such as SRCNN [1], FSRCNN [2], VDSR [3], SRGAN [4], BSRGAN [5], SwinIR [6], and Uniwin [7] are also being actively proposed.

When upscaling old broadcast content for full-screen display on high-resolution devices, SR technology must address the inherent challenges of enhancing low-quality,

low-resolution images. These images frequently contain significant sensor noise and blur, attributable to the limitations of camera technology during image acquisition. Applying SR under these conditions often amplifies or extends these distortions, resulting in an SR image of compromised quality. Recent SR methods like BSRGAN [5] and SwinIR [6] incorporate image enhancement techniques, including deblurring and denoising, to improve the perceptual quality of the resulting SR images. Therefore, in the evaluation of the quality of SR images, it is crucial to evaluate not only the extent of distortion but also the degree of improvement.

The field of Image Quality Assessment (IQA) provides methodologies for such evaluations. It is divided into Full-Reference (FR), Reduced-Reference (RR), and No-Reference (NR) IQA, depending on the availability of reference images. FR-IQA metrics, such as PSNR, SSIM [8], and LPIPS [9], leverage full reference images to assess image quality. In contrast, RR-IQA metrics, such as OSVP [10], REDLOG [11], and IGTS [12], use reduced reference images such as LR images or image patches. These reference-based metrics typically assume that the reference images, often high-quality originals, represent the highest standard of visual quality. They evaluate image quality based on the differences between the test image and the reference image, focusing solely on distortions in the test image and not accounting for potential improvements. On the other hand, NR-IQA metrics such as BRISQUE [13], NIQE [14], and DIIVINE [15] evaluate image quality without using reference images. Instead, they predict a visual quality based on Natural Scene Statistics (NSS) by measuring deviations from the general statistical characteristics observed in natural images. These methods focus primarily on detecting distortions and unnatural artifacts, often overlooking perceptual enhancements. As a result, these metrics face limitations when evaluating SR images that include both distortions and improvements. To evaluate SR images that encompass both distortions and improvements, new IQA metrics are needed, and an appropriate IQA dataset is essential for developing these metrics.

Most SR-IQA (i.e., IQA for SR images) datasets such as QADS [16], consist of high-quality original images, their SR counterparts, and corresponding quality scores. Specifically, LR images are generated by downsampling original images using various scaling factors (e.g., $\times 2$, $\times 3$, $\times 4$). As shown in Fig. 1 (a), the SR images are then obtained by upscaling LR images with various SR methods, using the same scaling factor used in the initial downsampling. This procedure ensures that the SR images match the original images in resolution, thereby enabling the computation of FR-IQA metrics. However, SR images generated with different scaling factors are not derived from the same original image, making fair comparison challenging. Additionally, information loss during the downsampling process complicates the analysis of the effects of the SR methods on image quality alone. Moreover, this experimental setup does not always align with

real-world scenarios. In practical applications, as shown in Fig. 1 (b), SR methods are applied directly to original LR images without a prior downsampling step. Thus, a reference image of the same resolution does not exist. To address this issue, Real-SRQ [17] captured pairs of LR and HR images of the same scene by adjusting the camera's focal length. However, since Real-SRQ focuses on pairs of high-quality captured images, it does not address the prevalent real-world challenge of applying SR to legacy content that is inherently low-quality (e.g., noisy, blurry). Consequently, a large-scale subjective dataset dedicated to the perceptual effects of SR on such challenging, low-quality source content is currently missing.

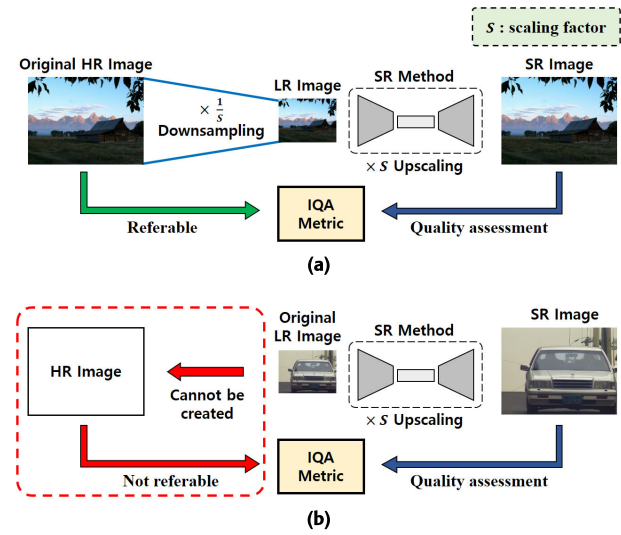


FIGURE 1. The scenarios of (a) existing SR research and (b) real-world environments on the application of SR and the quality evaluation of SR image.

It is also crucial to define the scope of this work in this specific context. Broadcast content is composed of video sequences, and various advanced Video Super-Resolution (VSR) approaches such as SCST [18], BF-STVSR [19], and VideoGigaGAN [20] have been actively proposed in recent years. However, our study deliberately concentrates on single-image SR. The primary contribution of this paper is the creation of a foundational dataset, and extending this task to VSR on low-quality sources introduces additional complexities, including the evaluation of temporal consistency and motion-related artifacts, which constitute substantial research challenge in their own right. We therefore posit that a robust public benchmark for the spatial quality of individual frames is a necessary prerequisite for the field before tackling the multifaceted challenge of spatio-temporal VSR quality assessment. Accordingly, this work concentrates on providing this essential, foundational resource.

In this paper, we propose a new SR-IQA dataset specifically for SR images of broadcast content, named

TABLE 1. Summary of SR visual quality assessment dataset.

Dataset	Year	Original Scenes	SR Methods	Scaling Factor	Distortion	Enhancement	Without Downsampling	SR Results	Subjective Evaluation	Subjects
Yang <i>et al.</i> [24]	2014	10	6	2, 3, 4	✓	✗	✗	540	ACR	30
Yeganeh <i>et al.</i> [25]	2015	13	8	2, 4, 8	✓	✗	✗	312	ACR	30
Ma <i>et al.</i> [26]	2016	30	9	2, 3, 4, 5, 6, 8	✓	✗	✗	1,620	ACR	50
SISRSet [27]	2019	15	8	2, 3, 4	✓	✗	✗	360	PC	16
QADS [16]	2019	20	21	2, 3, 4	✓	✗	✗	980	PC	100
SupER [28]	2019	14	19	2, 3, 4	✓	✗	✗	3024	PC	-
Real-SRQ [17]	2022	60	10	2, 3, 4	✓	✗	✓	1,620	PC	60
Konx [29]	2023	420	1	2, 4	✓	✗	✗	1,260	ACR	19
SRIJ [30]	2023	32	7	2, 3, 4	✓	✗	✓	608	ACR	43
SREB	2025	30	7	2, 4	✓	✓	✓	420	PC	51

Super-Resolution Enhanced Broadcasting content (SREB) dataset. Contrary to existing SR-IQA datasets, SREB utilizes the original images in their native resolution, without any prior downsampling. Moreover, the SR images are designed to consider both distortions and enhancements compared to the original content. We conducted a subjective quality test using a pairwise comparison (PC) method to obtain Mean Opinion Scores (MOSs) for SR images. We then performed an in-depth analysis of the subjective test results. Finally, existing IQA metrics were evaluated and compared using our dataset.

The main contributions of this study are outlined as follows:

- SREB dataset:** Our new dataset comprises original images, which are low-quality and low-resolution broadcast content, alongside their SR images, and associated quality scores. By applying SR methods that enhance or distort low-quality originals, SREB can be used to develop IQA metrics that reflect both distortions and enhancements in SR images. To reflect real-world scenarios, the original images were used at their native resolution without any prior downsampling. For the subjective quality assessment, these images were displayed in their actual size.
- Perceptual quality analysis:** We conducted a human study to analyze the perceptual quality characteristics of SR images, focusing on the effects of different SR methods and spatial resolutions. Additionally, we used a questionnaire to investigate the subjective factors perceived by human participants.
- Comparative evaluation of existing IQA metrics:** We compared the performance of ten NR-IQA metrics and two RR-IQA metrics on our dataset, clearly revealing the limitations and potential of existing IQA metrics. Based on these findings, the SREB dataset is expected to serve as a valuable resource for developing novel IQA metrics that jointly consider distortions and enhancements. Furthermore, IQA metrics developed using SREB are expected to be applicable not only to SR but also to various image enhancement tasks, such as deblurring, denoising, and high dynamic range (HDR) imaging.

The rest of the paper is structured as follows. Section II provides a comprehensive review of the existing literature on SR. In Section III, we detail the proposed dataset, while Section IV describes the subjective quality assessment conducted. Section V involves a comparative analysis of various image quality models utilizing our dataset. Finally, concluding remarks are given in Section VI.

II. RELATED WORK

IQA datasets are utilized to develop and benchmark image quality prediction models. Typically, they comprise a set of pristine original images, their distorted counterparts created with specific types and levels of distortion, and corresponding subjective quality scores, in the form of MOS. Notable IQA datasets include LIVE [21], VDID2014 [22], and MARFD [23].

Specifically, SR-IQA datasets are designed as benchmarks for SR-IQA metrics. They consist of original images, a variety of SR images generated using different methods and scaling factors, and associated subjective quality scores. Representative SR-IQA datasets include Yang *et al.* [24], Yeganeh *et al.* [25], Ma *et al.* [26], SISRSet [27], QADS [16], SupER [28], Real-SRQ [17], Konx [29], and SRIJ [30] which are summarized in Table 1.

Yang et al. used ten original images from BSD200 to generate 90 LR and 540 SR images, employing three scaling factors ($\times 2$, $\times 3$, $\times 4$) and six SR methods.

Yeganeh et al. included 13 original images at resolutions of 512×512 , spanning indoor and outdoor scenes, and generated 312 SR images using three scaling factors ($\times 2$, $\times 4$, $\times 8$) and eight interpolation methods.

Ma et al. extended the dataset of Yang *et al.* by modifying the LR image generation settings using the BSD200. There are 180 LR images using 30 original images and six scaling factors ($\times 2$, $\times 3$, $\times 4$, $\times 5$, $\times 6$, $\times 8$). The 1,620 SR images were generated using nine SR methods.

SISRSet comprised 15 original images, sourced from Set5, Set14, and BSD100. It used bicubic downsampling with three scaling factors ($\times 2$, $\times 3$, $\times 4$) to generate LR images, and eight SR methods were then applied to these LR images, producing a total of 360 SR images.



FIGURE 2. Exemplar original images of SREB dataset grouped by content characteristics: The images are displayed in a sequence from the first to the third row, each illustrating a distinct content group. Specifically, the image in the first row represents the ‘Person’ group, highlighting human subjects within the dataset. The second row features an image from the ‘Scene’ group, showcasing natural or urban environments. Finally, the third row displays an image from the ‘Screen Content’ group, focusing on digital or artificial scenes.

QADS selected 20 original images from the MDID [31] and created 60 LR images from original images, using three scaling factors ($\times 2$, $\times 3$, $\times 4$). It employed 15 traditional and six deep learning-based SR methods. Not all methods were applied across all scaling factors, resulting in a total of 980 SR images.

SupER contained 14 original images at a resolution of $2,040 \times 1,080$. A total of 3,024 SR images are generated using 19 SR methods and three scaling factors ($\times 2$, $\times 3$, $\times 4$). Additionally, subjective scores are obtained through PC using Amazon Mechanical Turk.

Real-SRQ captured both the original and LR images simultaneously using varying camera focal lengths to produce 60 original images and 180 corresponding LR images across three scaling factors. Applying ten different SR methods, the dataset includes a total of 1,620 SR images.

Konx is a cross-resolution IQA dataset with 420 images evaluated at three resolutions. It enables analysis of how perceived image quality changes with resolution and serves as a benchmark for training and evaluating NR-IQA models across different scales.

SRIJ is built using seven SR methods and consists of 608 SR images generated from 32 scenes cropped from [28], with alignment between LR and reference images. Most methods were applied at three scaling factors ($\times 2$, $\times 3$, $\times 4$). Subjective quality scores were collected through a single stimulus study.

However, existing datasets assume only distortions introduced by SR methods, failing to adequately reflect the quality improvements achieved by recent SR methods. In addition, most of these datasets use LR images generated through downsampling rather than raw LR images. This approach overlooks the practical challenges of dealing with genuinely low-quality, low-resolution images, such as those found in broadcasting.

III. PROPOSED DATASET

To reflect real-world scenarios where a full reference image for an SR image does not exist, SR methods should be directly applied to the original LR image without any downsampling.

Furthermore, while conventional SR methods have mainly focused on minimizing distortion that may occur during upsampling process, recent SR studies have made efforts to enhance image quality, where ‘enhancement’ primarily refers to the reduction of distortions present in the original image. Therefore, SR-IQA dataset needs to be designed to evaluate both distortions and enhancements induced by SR process. To this end, we introduce SREB, a new dataset that provides SR images reflecting these considerations. It also includes corresponding subjective quality scores obtained through a rigorous subjective quality assessment test.

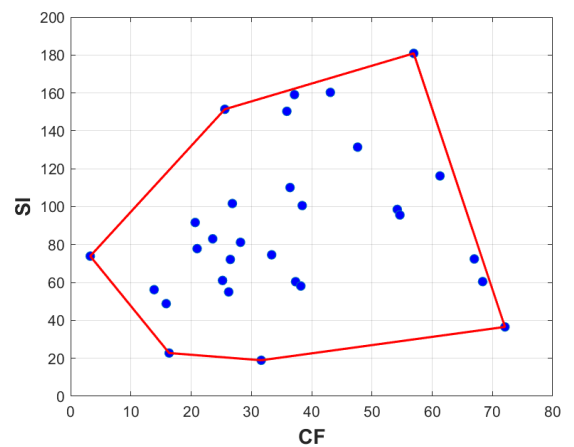


FIGURE 3. Scatter plot between spatial information (SI) and colorfulness (CF) for the 30 original images in the SREB dataset.

A. CURATION OF ORIGINAL IMAGES

We attempt a new approach, different from the existing dataset, in constructing an SR-IQA dataset from low-quality original images. In the real-world scenario, original images with high perceptual quality often do not exist due to the limitations of photographing device and applied compression. Therefore, it is preferable to use low-quality broadcasting content as the original images in the dataset. Considering this, the method of obtaining the low-quality original image is as follows.

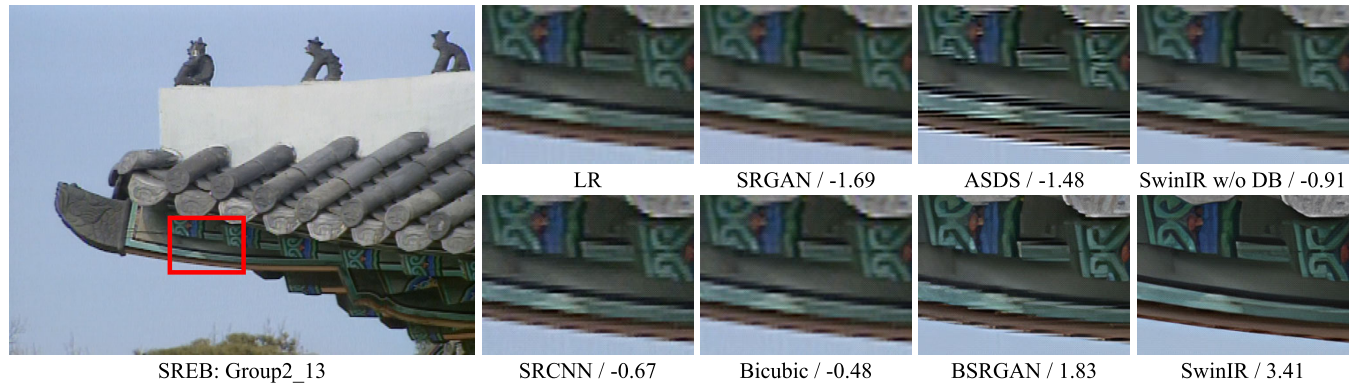


FIGURE 4. Visual comparison of various SR methods for $\times 2$ scaling factor on SREB dataset and MOS corresponding to each SR image.

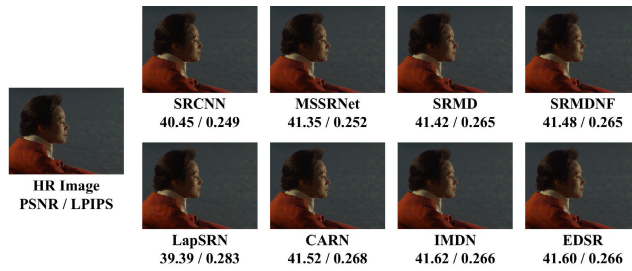


FIGURE 5. Visual comparison of various SR methods for $\times 4$ scaling factor on SREB dataset and PSNR, LPIPS corresponding to each SR image.

Original videos were obtained from broadcast content of the Korean terrestrial video station SBS between 1995 and 2007, with each video clip being 7-10 seconds long. To take into account a variety of characteristics of broadcast content, we divided them into drama, documentary, and entertainment categories, selecting a total of six programs, with two in each category. The 20 video clips, selected evenly from six programs, were de-interlaced, cropped, and resized to convert the original $720 \times 512i$ resolution to $720 \times 540p$. These essential preprocessing steps were performed to convert the original interlaced broadcast content into a standardized progressive format, while carefully minimizing any adverse effects on image quality. Specifically, for de-interlacing, the original $720 \times 512i$ video clips were converted to progressive scan to mitigate “combing” artifacts common in interlaced video. To this end, the Yet Another Deinterlacing Filter (YADIF) [32] method was employed. YADIF is a motion-adaptive de-interlacer, chosen specifically to minimize quality degradation and preserve inherent visual information during this conversion, particularly in scenes with motion. Following de-interlacing, cropping removed irrelevant black bars, ensuring only primary content remained while maintaining the effective aspect ratio. Subsequently, the resolution was standardized to $720 \times 540p$ through a resizing process designed to avoid introducing new artifacts. These methodical preprocessing steps ensured the dataset is built upon a artifact-free progressive video base, suitable for subsequent SR processing and quality assessment. Following

these process, we initially selected 93 candidate images were selected from the video clips to cover a wide range of texture, structure, motion, and other characteristics.

To ensure the diversity of scene properties in the SREB dataset, we assessed each image based on spatial information (SI) [33] and colorfulness (CF) [34]. These indices were calculated to gauge the spatial complexity and color diversity of image. SI is defined as follows:

$$SI = \sigma[Sobel(I_F)], \quad (1)$$

where I_F denotes the luminance component of image, $Sobel(\cdot)$ denotes the Sobel filter, and σ represents the standard deviation. CF is defined as follows:

$$rg = I_R - I_G, \quad (2)$$

$$yb = \frac{1}{2}(I_R + I_G) - I_B, \quad (3)$$

$$\sigma_{rgyb} = \sqrt{\sigma_{rg}^2 + \sigma_{yb}^2}, \quad (4)$$

$$\mu_{rgyb} = \sqrt{\mu_{rg}^2 + \mu_{yb}^2}, \quad (5)$$

$$CF = \sigma_{rgyb} + 0.3 \times \mu_{rgyb}, \quad (6)$$

where I_R , I_G , I_B denote the red, green, and blue components of the image, respectively, and σ and μ denote the standard deviation and mean values. According to the calculated SI and CF values, 30 images were selected by excluding those with overlapping characteristics. For the diversity of content and texture, we categorize the original images into three groups: person (row 1), scene (row 2), and screen content (row 3), as shown in Fig. 2. In Fig. 3, the 30 selected original images encompass a comprehensive range of spatial and color complexity, effectively representing degree of monotony, normality, and complexity.

B. DESIGN OF SUPER-RESOLUTION IMAGE SET

The SR process for the selected 30 original images bypasses downsampling to directly apply SR methods. This approach ensures that the assessment reflects actual performance without the quality alteration caused by downsampling, simulating real-world application scenarios.

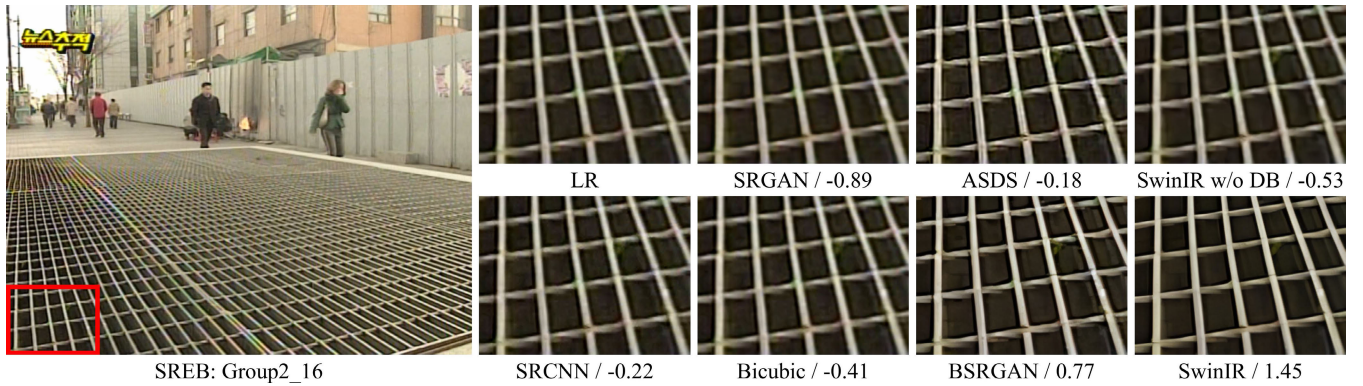


FIGURE 6. Visual comparison of various SR methods for $\times 2$ scaling factor on SREB dataset and MOS corresponding to each SR image.

TABLE 2. CNN-based SR method results (PSNR, SSIM and LPIPS between HR and SR image).

Method	PSNR \uparrow	SSIM \uparrow (0 - 1)	LPIPS \downarrow
LapSRN [35]	30.79	0.905	0.169
SRCCN [1]	29.57	0.880	0.159
MSSRNet [36]	30.57	0.902	0.143
SRMD [37]	30.87	0.905	0.139
SRMDNF [37]	31.02	0.909	0.138
CARN [38]	31.14	0.911	0.144
IMDN [39]	31.21	0.913	0.138
EDSR [40]	31.49	0.926	0.132

To ensure a comprehensive and diverse SR IQA dataset, we selected several SR methods to represent a range of approaches. We began by including Bicubic interpolation, the most conventional and widely-recognized baseline for SR tasks. Next, to represent classical machine learning approaches that predate deep learning, we included the example-based method ASDS [41]. This ensures our dataset covers techniques beyond simple interpolation and captures a wider range of SR characteristics.

To select a representative CNN-based method, we performed a comprehensive analysis on eight methods, with results detailed in Table 2 and Fig. 5. Our evaluation indicated a high degree of overall similarity across the methods when applied to our low-quality sources. We observed minimal variations in all evaluated quality metrics, including those for PSNR, SSIM and LPIPS. This observation was further supported by our qualitative visual assessment, which revealed no discernible differences. Given this consistent evidence of redundancy, we selected only the well-known SRCCN as a representative from this category. This decision was made not only to avoid subject fatigue but also to establish a low-quality anchor, thereby ensuring a clearer perceptual distinction between the other methods in our subjective study.

To make our dataset more diverse and show different levels of image quality, we also included GAN-based SR methods, specifically SRGAN and BSRGAN. While GAN-based

TABLE 3. Seven SR methods used for generating SR images in the SREB dataset.

Method	Type	Year	Scaling Factor	Images
Bicubic	Interpolation	-	2, 4	60
ASDS [41]	Example based	2011	2, 4	60
SRCCN [1]	CNN	2014	2, 4	60
SRGAN [4]	GAN	2016	2, 4	60
BSRGAN [5]	GAN	2021	2, 4	60
SwinIR [6]	Transformer	2021	2, 4	60
SwinIR w/o DB	Transformer	2022	2, 4	60

methods often generate perceptually convincing results, they may exhibit lower fidelity to the ground truth. We selected SRGAN as a method representative of outcomes where distortions are amplified, often resulting in images perceived as having lower quality than the original LR input. On the other hand, BSRGAN was chosen as a method that creates perceptually better-quality images. This allows our dataset to cover the full range of SR outcomes, from those with reduced quality to those with improved visual appeal.

Additionally, to represent the latest SR technologies, we included Transformer-based SR methods, namely SwinIR and its version without deblurring (SwinIR w/o DB). These methods use image restoration techniques to handle complex damage and have shown excellent performance. Similar to our GAN-based selection, SwinIR w/o DB was included to show cases where the SR output might have lower quality than the original, while SwinIR was chosen to demonstrate significant quality improvements. This ensures our dataset includes the newest technologies and various types of SR methods, providing a complete reference point that covers both quality degradation and enhancement scenarios for future research. The process of generating the SR image can be defined as follows:

$$I_{SR} = (I_{LR}) \uparrow_s, \quad (7)$$

$$I_{LR} = I * d_1 + d_2 + \dots, \quad (8)$$

where I_{LR} is original LR image, \uparrow_s denotes SR with a scaling factor of s , I is pristine image, and d_n represents different

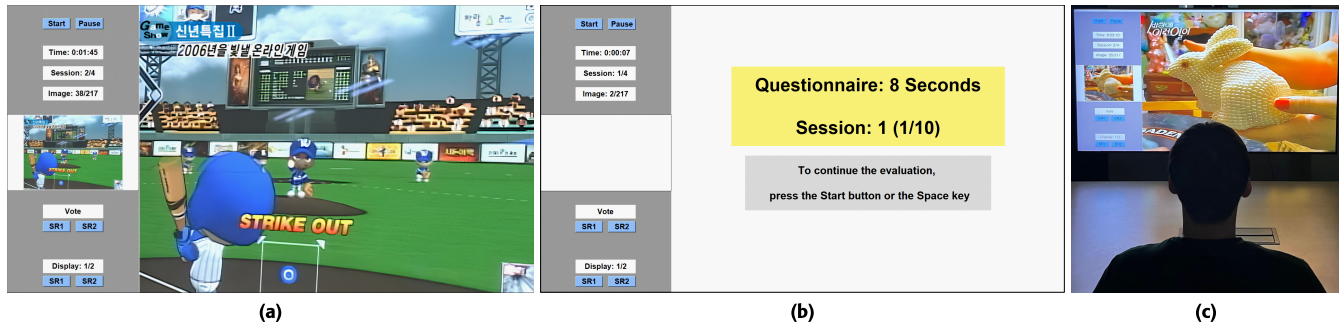


FIGURE 7. (a) The GUI for the pairwise comparison test. The left panel displays session information, the original LR image for reference, and control buttons. The right panel displays one of the SR images being compared. (b) Questionnaire screen on the GUI; For each survey, a maximum of 8 seconds is given, and the session and survey number are displayed. Subjectives select one primary reason they perceive unselected image to have poor quality from Table 4 and record it on the provided questionnaire. (c) Scene of subjective assessment.

kinds of distortion, such as blur and noise, that inherently contained in I_{LR} . In our study, I_{LR} was not synthesized but acquired with distortion included. The images were processed using scaling factors of $\times 2$ and $\times 4$, resulting in SR images with resolutions of 1440×1080 and 2880×2160 . A total of 420 SR images (30 images $\times 7$ methods $\times 2$ scaling factors) were generated. Table 3 summarizes the type, SR method, scaling factor, and the number of images. Additionally, Fig. 4, Fig. 6 shows the example of generated SR images along with their respective MOS obtained from the test described in Section IV. LR image exhibit blurring and discontinuous edges, which can be either improved or deteriorated by SR. For instance, SRGAN was evaluated with a low MOS due to the amplification of such distortions, whereas SwinIR received a high MOS as the image quality was enhanced.

IV. SUBJECTIVE QUALITY ASSESSMENT

A. SUBJECTIVE STUDY DESIGN

In the previous subjective studies on SR images such as [24], [25], [26], and [29] the Absolute Category Rating (ACR) [33] was often adopted as the subjective evaluation method. In ACR, the subject views one test image at a time and evaluates its quality using a discrete categorical scale. However, this protocol has limitations in distinguishing subtle quality differences among SR images produced by different SR methods. To address this, recent subjective studies such as [16], [17], [27] have adopted the Pairwise Comparison (PC) method, as shown in Table 1. This method allows subjects to easily recognize subtle quality difference by selecting the one that they perceive to have superior visual quality from a pair of SR images. Therefore, in this study, we employed the PC method to conduct a subjective quality assessment of SR images. Our evaluation method and environment were established in accordance with ITU-R Rec. BT500 [42].

1) GUI CONFIGURATION

For our subjective quality test, we implemented a Graphical User Interface (GUI) designed for the PC method, which is shown in Fig. 7 (a). The GUI comprises four main sections:

Top-left displays evaluation progress—test running time, the count of comparison executed, and session information—with start/pause controls.

Middle-left shows the original LR image for reference to identify changes in SR images.

Bottom-left features voting and display switch buttons for two SR images.

Right presents a single SR image, with options to toggle between two SR images for comparison. This facilitates easier comparison for the subject.

Interaction with the GUI is keyboard-friendly, facilitating efficient comparison and selection processes. Subjective experiments were conducted on a Samsung 65-inch 4K UHD TV. The viewing distance was set to 1.6 times the display height and the peak luminance of the display was set to 200 cd/m^2 , as specified in ITU-R Rec. BT500 [42]. Original LR and corresponding SR images are shown at their actual resolutions, 720×540 for LR, and 1440×1080 ($\times 2$) or 2880×2160 ($\times 4$) for SR images. This allowed for considering only the impact of SR methods in subjective image quality assessment with the same scaling factor and enabled the analysis of human perceptual systems based on resolution with different scaling factors. Fig. 7 (c) illustrates the evaluation of SR images using our GUI.

2) COMPARISON PAIRS AND EVALUATION SESSIONS

To conduct PC-based evaluation, SR images for the same content are paired in sets of two. Each source content was processed using seven different SR methods with two scaling factors, yielding seven SR images at both $\times 2$ and $\times 4$ scaling factors. Thus, each source content has 21 pairs ($7C_2 = 21$) for comparison at each scaling factor. Additionally, 49 pairs ($7 \times 7 = 49$) were generated for cross-scaling factor comparisons ($\times 2$ vs. $\times 4$). Therefore, for a single source content, there are a total of 91 comparison pairs ($21 + 21 + 49 = 91$). With 30 source content in total, the overall number of comparison pairs amounts to $2,730$ ($91 \times 30 = 2,730$).

A total of 51 subjects with normal visual acuity (13 females and 38 males), aged between 20 and 45 years, participated in our subjective quality assessment test. All subjects provided consent for participation in this test. Written informed

consent was obtained from all participants prior to their involvement. All procedures involving human participants were exempt from review by the Hanyang University Institutional Review Board (IRB) under Application No. HYUIRB-202102-012. We divided the 51 subjects into three equal groups, with each group assessing SR images for ten distinct source content. As a result, each participant conducted a total of 910 votes ($91 \times 10 = 910$). In total, we collected 46,410 votes ($910 \times 51 = 46,410$) from all 51 subjects.

The test was structured into four sessions: the first two sessions focused on comparisons in the same $\times 2$ or $\times 4$ scaling factor, respectively, while the final two sessions compared images across two scaling factors. The last two sessions aimed to investigate how scaling factors and resolution differences affect perceived image quality. The results from the first and second sessions were used to compute MOS for $\times 2$ and $\times 4$ scaling factors, respectively, while the results from all four sessions were combined to compute MOS for the integrated $\times 2$ and $\times 4$ scaling factors (i.e., $\times 2 \times 4$). To mitigate visual fatigue, we limited sessions to 30 minutes and incorporated a 5-minute break between each. On average, subjects completed the experiment in 98 minutes.

3) SURVEY

To further explore the distortion factors in SR images, we conducted a survey during a subjective experiment. Subjects were given a questionnaire before they started the evaluation. During the assessment, a questionnaire screen appears on the GUI with a probability of 1 in 20 after each voting, as illustrated in Fig. 7 (b). If the questionnaire screen popped up, subjects were asked to identify the primary reason for the poor quality of the non-selected image from the previous pair. This process aimed to pinpoint the primary causes of distortion in the non-selected images. The questionnaire's components are detailed in Table 4, with the resolution factors only used in the 3rd and 4th sessions to compare SR images at varying scaling factors.

TABLE 4. Questionnaire items for distortion factors in SR images.

Factors	ID	Reasons
Noise	1	The image is not clean and contains noise.
Blur	2	The image is not clear and blurry.
Detail	3	Distorted patterns, shapes, or edges are present.
Color & Brightness	4	There is unnatural color distortion.
Resolution	5	Brightness level is either too dark or bright.
	6	High resolution causes visual unnaturalness.
	7	Low resolution causes visual unnaturalness.

4) CHECKPOINT

For the identification and elimination of outliers, we introduced checkpoint comparison pairs in each session. These pairs consist of SR images generated with SwinIR and their Gaussian-blurred counterparts. This setting ensures

clear differences in image quality, allowing verification of subjects' faithful engagement in the subjective experiments and the evaluation of the results' reliability. A total of 20 checkpoints have been added, and if an subject provides incorrect responses in two or more checkpoints, they were considered as outliers and excluded from the results. In our test, all 51 subjects passed the checkpoints.

5) TRAINING SESSION

Before the subjective image quality assessment, all subjects underwent a training session. This session covered evaluation procedures, GUI navigation, and questionnaire completion. They also engaged in hands-on practice with the GUI, evaluating dummy SR images produced in the same manner to those in Section III, using four source content not included in the SREB dataset.

6) BIAS MITIGATION STRATEGIES

To ensure the reliability and validity of our subjective quality assessment, several measures were implemented to mitigate potential biases. First, the choice of the PC method over ACR reduces scale-usage and memory biases, a point introduced at the beginning of Section IV-A. Second, a mandatory training session was conducted for all participants to minimize procedural bias, with the full procedure detailed in Section IV-A5. Third, to prevent visual fatigue, sessions were limited in duration with enforced breaks, following the methodology described in Section IV-A2. Finally, we embedded checkpoint pairs to identify and filter out unreliable observers, directly addressing subject reliability bias as explained in Section IV-A4. The successful validation of all 51 subjects through these checkpoints underscores the high reliability of our collected data.

B. POST-PROCESSING FOR SUBJECTIVE SCORES

The voting results obtained from PC-based subjective test cannot be directly used as subjective quality scores. Thus, MOSs were derived through post-processing methods. We used the Bradley-Terry (B-T) method [43], a probabilistic model commonly used for PC results. The MOSs were estimated via Maximum Likelihood Estimation (MLE), as described in [17]. Specifically, in a pair of i and j , C_{ij} represents the number of times i beats j , expressed as follows:

$$C_{ij} = \begin{cases} \text{The number of times } i \text{ beats } j, & i \neq j \\ 0, & i = j. \end{cases} \quad (9)$$

In our study, for a pair of SR images i and j , C_{ij} represents the total number of times image i was selected as being of higher quality than image j , aggregated across all subjects. The B-T model is the probability of i beats j , expressed as follows:

$$P_{ij} = \frac{e^{q_i}}{e^{q_i} + e^{q_j}}. \quad (10)$$

Here, $Q = \{q_1, q_2, \dots, q_N\}$ represents estimated subjective quality score, i.e., MOS, of each image, and our goal is to

estimate Q using MLE. The likelihood $P(D|Q)$ represents the probability of the voting results D as follows:

$$P(D|Q) = \prod_{i=1}^N \prod_{\substack{j=1 \\ j \neq i}}^N (P_{ij})^{C_{ij}}. \quad (11)$$

For the convenience of calculations, negative log likelihood $L(Q)$ can be expressed as Eq. (12) and minimized.

$$L(Q) = - \sum_{i=1}^N \sum_{\substack{j=1 \\ j \neq i}}^N C_{ij} \log (P_{ij}). \quad (12)$$

Using condition $\partial L(Q)/\partial q_k = 0$, Q can be derived as in Eq. (13).

$$q_k^{t+1} = \log \left(\frac{\sum_{j=1}^N C_{kj}}{\sum_{i=1}^N \frac{C_{ki} + C_{ik}}{e^{q_k^t} + e^{q_i^t}}} \right), \quad k = 1, 2, \dots, N, \quad (13)$$

where t represents the number of iterations. By initializing with $Q = \{1, 1, \dots, 1\}$ and iteratively updating Q based on the voting results until it converges, MOS of each SR image can be obtained. To ensure stable MOS estimation during the iterative update process, the predicted scores are normalized by subtracting the mean, resulting in a zero-mean distribution.

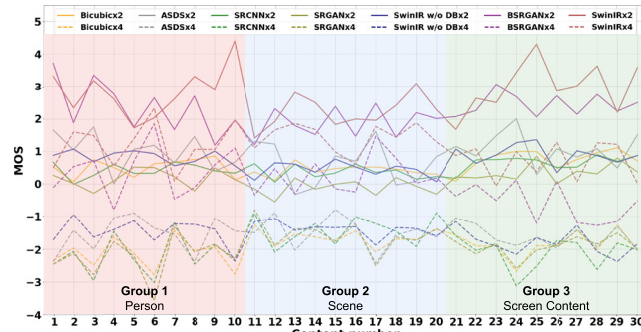


FIGURE 8. $\times 2 \times 4$ MOS score of content by all SR methods. The solid line represents the $\times 2$ scale and the dotted line represents the $\times 4$ scale.

TABLE 5. Summary of the MOS for SR images on SREB dataset.

Scaling Factor	SR Images	Max	Min	Average
$\times 2$	210	4.61	-3.27	
$\times 4$	210	4.44	-2.35	0
$\times 2 \times 4$	420	4.39	-3.57	

C. STUDY ON THE SUBJECTIVE QUALITY TEST RESULTS

1) MOS ANALYSIS

The SREB dataset provides MOSs for 420 SR images, with the MOS for each SR image calculated using voting results from the same source content. As a result, 210 MOSs were obtained for each of $\times 2$ and $\times 4$, respectively. In addition, a total of 420 MOSs were further obtained for $\times 2 \times 4$. These results are summarized in Table 5. For the comparison of the

SR methods and the analysis of the MOS trend by group, the MOS for $\times 2 \times 4$ scaling factor of each method for each content is shown in Fig. 8. Each color represents the SR method, with $\times 2$ scale represented by a solid line and $\times 4$ scale by a dotted line. The graph shows a consistent trend of better SR quality at lower scaling factors across all methods. The graph can be divided into four parts:

1. The first part includes the $\times 2$ scale methods (solid line) located in the 2 to 4 score range. BSRGAN and SwinIR of the $\times 2$ scale showed better results compared to other methods, improving the SR image quality in terms of human perceived quality.
2. The second part includes the $\times 2$ scale methods located in the -1 to 2 score range. These methods failed to mitigate the artifacts present in the low-quality source images. Moreover, they often amplified these distortions, leading to a degradation in perceptual quality and thus lower MOS scores.
3. The third part includes the $\times 4$ scale methods (dotted line) located in the -1 to 2 score range. BSRGAN and SwinIR at the $\times 4$ scale maintained the MOS score by removing the blur and noise factors, although the performance of restoring detailed information decreased as the scaling factors increased. However, BSRGAN's performance is partially poor in the screen content group (21-30), showing a low MOS score.
4. The last part includes the $\times 4$ scale methods located in the -3 to -1 score range. As with the previous $\times 2$ scale methods, they not only amplify the distortion of the original but also show a greater decline in performance compared to BSRGAN and SwinIR due to the increased scaling factor.

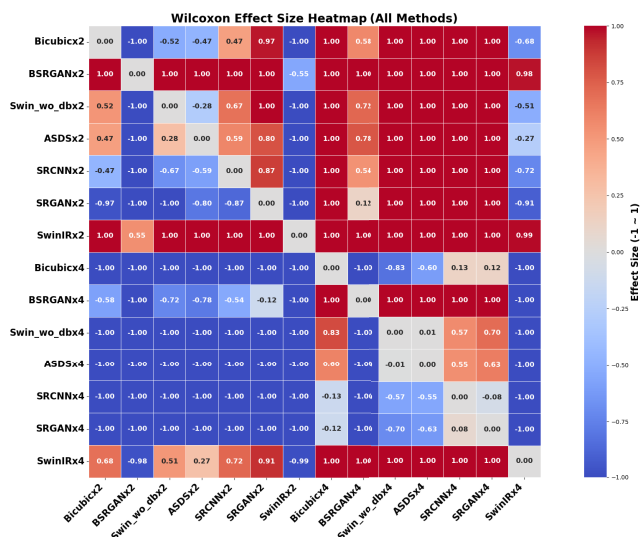


FIGURE 9. The effect size results based on the Wilcoxon signed-rank test are plotted within the range of -1 to 1, where values closer to 1 indicate that the method in the row shows better performance, while values closer to -1 indicate that the method in the column performs better. A value of 0 indicates no significant performance difference between the two methods.

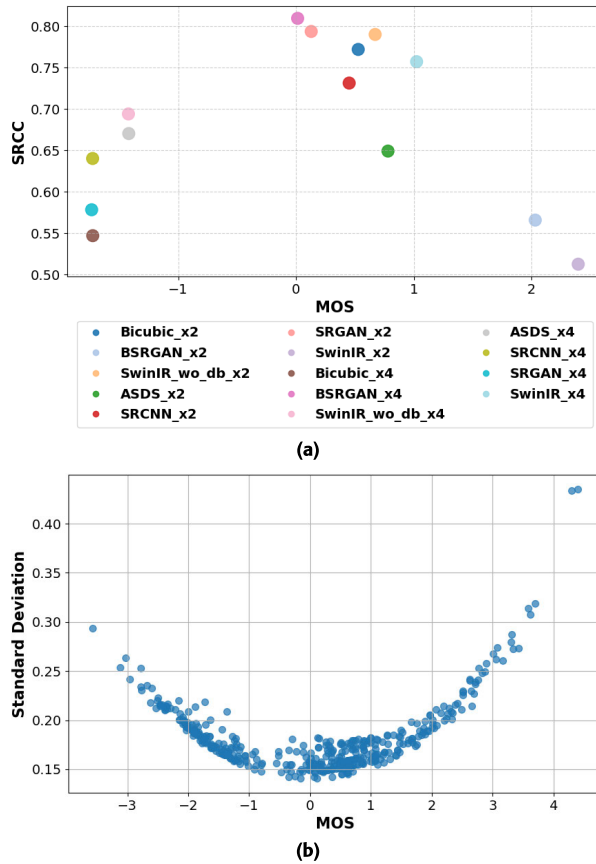


FIGURE 10. Distributions of distortion for (a) Overall SR images and (b) based on scaling factor on SREB dataset.

To describe this grouping, we assess the statistical significance of performance differences among methods using the Wilcoxon signed-rank test [44]. This non-parametric test is appropriate because we are comparing the performance of different SR methods on the same set of source images, meaning the data consists of paired samples. Effect size is further computed to quantify the magnitude of these differences. As shown in Fig. 9, the performance differences are visualized via effect size. For example, when comparing Bicubic $\times 2$ against other methods, the resulting effect sizes span a wide range from -1 to 1 . This demonstrates that the SREB dataset includes methods with significantly varying performance levels, confirming its suitability as a comprehensive benchmark for advancing SR-IQA metric development.

2) CONSISTENCY ANALYSIS OF SUBJECTS' EVALUATIONS

To assess the consistency of subjects' evaluations, two types of results are presented in Fig. 10. Fig. 10 (a) presents the mean MOS of each SR method along with the mean SRCC across subjects for each method based on voting results. SR methods with extreme MOS exhibited lower subject consistency, with SRCC around 0.5, whereas methods with mid-range MOS showed higher consistency, with SRCC close to 0.8. This indicates that subjects' judgments diverged

more for SR methods producing either very high or very low image quality.

Fig. 10 (b) illustrates the MOS of SR images along with their standard deviations. A similar trend is observed: SR images with extreme MOS exhibited higher standard deviations, suggesting greater variability in subjects' evaluations of the same stimuli. This finding contrasts with the trend typically reported for artificially distorted or compressed image datasets, where standard deviations are usually lower at the extremes of MOS and higher in the mid-range. Nevertheless, the standard deviations in SREB are relatively lower compared to those reported in other datasets, implying a higher overall consistency in subjective evaluations. This relative consistency is noteworthy, but variations across SR methods require further analysis.

Such differences may stem from the diversity of degradation types and enhancement mechanisms inherent in SR. For example, when comparing severely degraded images, some dominated by noise and others by blur, subjects may differ in their preferences. In addition, although certain SR methods effectively reduce noise and blur, they can simultaneously remove original textures or introduce novel artifacts. As a result, subjects must weigh the perceived improvements against the newly introduced distortions, leading to divergent opinions. These observations suggest that in SR method development, it is not sufficient merely to address degradations; it is also critical to minimize unnatural artifacts introduced during the enhancement process.

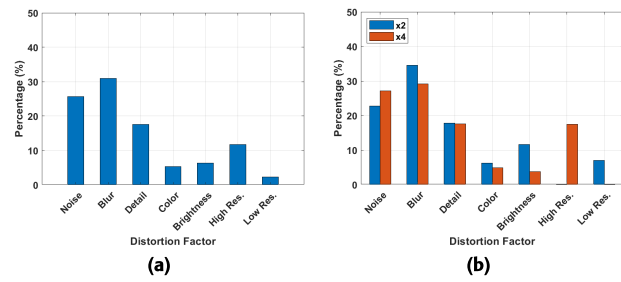


FIGURE 11. Distributions of distortion for (a) Overall SR images and (b) based on scaling factor on SREB dataset.

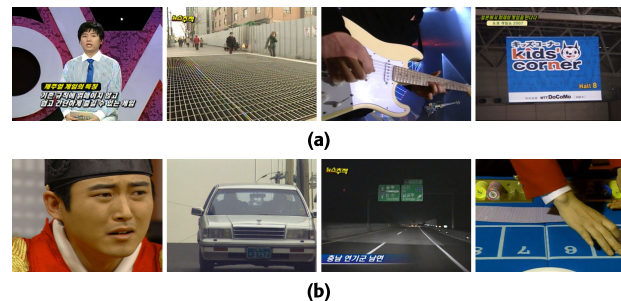


FIGURE 12. Content dominated by (a) blur distortion and (b) noise distortion when SR is applied.

3) DISTORTION ANALYSIS

Based on the subjects' questionnaire responses, we analyzed primary distortion types. The distribution of distortion for

all SR images is illustrated in Fig. 11 (a), with blur being the most dominant, followed by noise and loss of detail. Although SR typically induces blur rather than noise, noise from original low-quality broadcast content was found to be amplified in SR images, negatively affecting quality. Therefore, accurately evaluating blur and noise is critical for developing objective quality metrics for SR images from low-quality content. Fig. 11 (b) represents the distribution of distortion based on scaling factors. Both scaling factors of $\times 2$ and $\times 4$ show that blur and noise are predominant, followed by detail. The noise ratio increased in $\times 4$ compared to $\times 2$. This is because the higher resolution allows for clearer identification of finer details in the image, thereby making noise easier to recognize. Notably, in the $\times 4$ scaling factor, high resolution was chosen as the fourth most frequent factor at 17.48%. This is due to existing distortions being amplified as the scale increases, resulting in an overall degradation in quality.

Additionally, we conducted an analysis of distortions for each content. In Fig. 12 (a), it depicts instances where blur was predominantly selected as the primary distortion over noise. These images typically contain high levels of texture and edges, making noticeable areas of blur generated when SR is applied. The influence of blur on the sharpness of patterns and edges is evident, negatively affecting the overall image quality. Conversely, content where noise was overwhelmingly chosen as the main distortion over blur is depicted in Fig. 12 (b). These images are often characterized by simplicity and lack of texture, making noise more noticeable than blur within the images. Such content-specific distortion tendencies can help develop more effective IQA metrics.

V. EVALUATION OF OBJECTIVE IQA MODELS

In this section, we evaluate and compare the performance of existing IQA metrics on our SREB dataset.

A. TEST IQA MODELS AND EVALUATION METRICS

Since only original LR images were available, we tested NR and RR IQA methods on the SREB dataset. Specifically, ten NR IQA metrics were employed: BIQAA [45], BRISQUE [13], BLIINDS II [46], SRmetric [26], HyperIQA [47], TRes [48], MANIQA [49], KLTSRQA [17], ReIQA [50] and ARNIQA [51]. Additionally, two RR-IQA methods were employed: OSVP [10], REDLOG [11]. For RR-IQA evaluation, LR images containing only partial information from the perspective of the SR images were used as reduced references.

BIQAA [45] predicts the quality of images by measuring the variability in expected image entropy. BRISQUE [13], an NSS-based model, quantifies naturalness to predict quality scores using the Mean Subtracted Contrast Normalized (MSCN) coefficient along with Generalized Gaussian Distribution (GGD) and Asymmetric Generalized Gaussian Distribution (AGGD) calculations. BLIINDS II [46] is

a Bayesian inference model that predicts image quality using NSS models of Discrete Cosine Transform (DCT) coefficients, which enables simple learning and quality score prediction through feature extraction and probabilistic modeling. SRmetric [26] combines local, global frequency, and spatial features using Principal Component Analysis (PCA) and steerable wavelet decomposition for quality prediction through regression modeling. HyperIQA [47] simulates how human evaluate an image, enabling the network to recognize image content and adaptively adjust parameters for quality score prediction. TRes [48] integrates global and local features using CNNs and Transformers for feature extraction and score prediction. On the other hand, MANIQA [49] utilizes ViT for feature extraction and enhances the interaction between global and local image regions using modules that account for channel and spatial dimensions, predicting the final score with dual branches for each patch. KLTSRQA [17], a Karhunen-Loeve Transform (KLT)-based model, uses AGGD parameters and coefficient energy to extract image characteristics and predict quality. ReIQA [50] and ARNIQA [51] introduce various distortions to pristine images to train the feature extractor on diverse distortion types, employing contrastive learning to enhance performance in image quality assessment by increasing correlation among identical distortions across different content. One of the RR-IQA methods, OSVP [10], utilizes features that represent directional relationships with the surrounding regions of an image. It compares the features of a reduced reference image with those of a test image to calculate a quality score. REDLOG [11] evaluates image quality by using the difference in entropy of Discrete Wavelet Transform (DWT) coefficients between a reduced reference image and a test image.

The objective of IQA metrics is to achieve high correlation with MOS. To evaluate the performance, we employed Pearson Linear Correlation Coefficient (PLCC), Spearman Rank Correlation Coefficient (SRCC), and Root Mean Square Error (RMSE), which represent prediction accuracy, monotonicity, and error, respectively. Higher correlation with MOS is indicated by PLCC and SRCC values closer to 1, and an RMSE closer to 0.

To conduct the evaluation, 5-fold cross-validation was utilized, with the SR images randomly split into 80% for the training set and 20% for the test set. Throughout 1000 iterations, we ensured random partitioning of the training and test sets in each iteration. For all experimental results obtained from these 1000 train-test repetitions, average values were used as final performance indices. Among the learning-based IQA models, those that extract features and utilize regressors adopted the Support Vector Regressor (SVR). ARNIQA utilized a pretrained encoder to extract features from the SREB dataset and trained a regressor using these features. To introduce nonlinearity to the predicted scores, we fitted them to MOS using the same non-linear logistic function when calculating PLCC and RMSE. The logistic function is

TABLE 6. Test results for various IQA metrics on the SREB dataset.

Method	PLCC	$\times 2$		PLCC	$\times 4$		PLCC	$\times 2 \times 4$	
		SRCC	RMSE		SRCC	RMSE		SRCC	RMSE
NR	BIQAA [45]	0.209	0.241	1.621	0.176	0.174	1.315	0.280	0.358
	BRISQUE [13]	0.876	0.805	0.776	0.871	0.714	0.644	0.865	0.820
	BLIINDS II [46]	0.820	0.709	0.921	0.848	0.700	0.686	0.779	0.748
	SRmetric [26]	0.872	0.793	0.793	0.867	0.725	0.652	0.891	0.828
	HyperIQA [47]	0.738	0.720	1.574	0.720	0.740	1.288	0.802	0.795
	TRes [48]	0.810	0.781	1.260	0.703	0.653	1.189	0.759	0.748
	MANIQA [49]	0.821	0.664	1.097	0.829	0.710	0.861	0.844	0.808
	KLTSRQA [17]	0.910	0.861	0.697	0.874	0.724	0.661	0.891	0.858
	ReIQA [50]	0.880	0.807	0.769	0.864	0.703	0.657	0.933	0.899
RR	ARNIQA [51]	0.915	<u>0.860</u>	0.652	0.889	0.777	0.598	0.935	0.900
	OSVP [10]	0.669	0.693	1.639	0.673	0.470	1.321	0.178	0.144
	REDLOG [11]	0.810	0.734	0.948	0.793	0.616	0.793	0.626	0.576

defined as follows:

$$f(x) = \frac{\lambda_1 - \lambda_2}{1 + \exp\left(\frac{-x+\lambda_3}{|\lambda_4|}\right)} + \lambda_2, \quad (14)$$

where x represents the predicted score, $f(x)$ represents the fitted predicted score, and λ_k ($k = 1, 2, 3, 4$) are parameters aimed at minimizing the mean square error between $f(x)$ and MOS.

B. COMPARATIVE TEST RESULTS

The evaluation results of the existing metrics on the SREB dataset are presented in Table 6. BIQAA failed to accurately predict perceptual image quality. This metric considers the orientation of images, which can vary significantly depending on the content rather than the quality characteristics. In addition, REDLOG and OSVP failed to capture quality changes according to scaling factors, leading to significant performance degradation at $\times 2 \times 4$ scaling factor. Furthermore, BLIINDS II, HyperIQA, TRes, MANIQA did not exhibit robust performance in assessing SR images generated from low-quality broadcast content. Even the recently proposed deep learning-based models such as HyperIQA, TRes, and MANIQA failed to achieve a PLCC of 0.85 or higher for all scaling factors. In contrast, the NSS-based model BRISQUE demonstrated PLCCs of at least 0.86, with the RMSE being the second lowest at $\times 4$ with a value of 0.644. SR-IQA models like SRmetric and KLTSRQA also exhibited good performance by achieving PLCCs of at least 0.86 across all scaling factors. Notably, KLTSRQA achieved the best SRCC of 0.861, and the second-best PLCC and RMSE of 0.910 and 0.697, respectively, at $\times 2$.

ARNIQA and ReIQA, which learn degradation representations using contrastive learning, demonstrated outstanding performance at $\times 2 \times 4$. However, ReIQA exhibited a noticeable drop in performance at both $\times 2$ and $\times 4$, suggesting that further improvement is needed for single-scale quality prediction. In particular, ARNIQA achieved the best performance across all scales except for SRCC at $\times 2$. Both methods jointly used original and half-scale images during training, enabling robustness to scale variations and resulting

in high performance at $\times 2 \times 4$. These results highlight that contrastive learning, recently introduced to IQA, is effective in representing image quality. They also suggest that combining contrastive learning with scale-aware training is a promising direction for future SR IQA development.

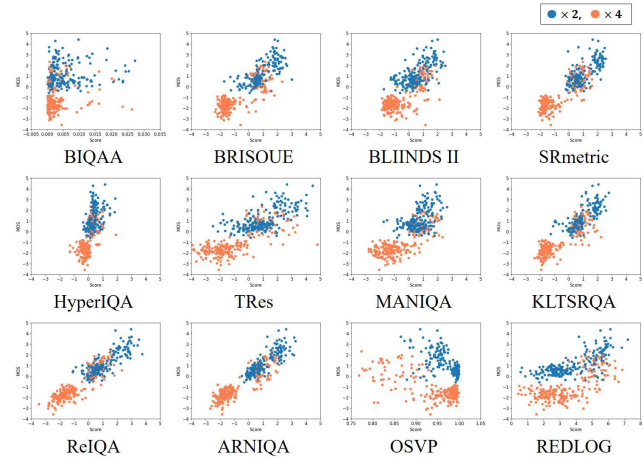


FIGURE 13. Scatter plots of predicted scores from various IQA metrics for $\times 2 \times 4$ MOS on the SREB dataset.

Fig. 13 shows the scatter plots between $\times 2 \times 4$ MOS of SREB and the predicted scores by each metric. To visualize the direct relationship, the predicted scores are plotted without logistic fitting. BIQAA and OSVP show a widely scattered distribution due to its inconsistency with MOS. In particular, OSVP shows a negative correlation between prediction scores and MOS. This is because OSVP evaluates image quality based on the similarity between the SR image and the original image, and in the SREB dataset, high-quality SR images tend to have a greater difference from the low-quality original images. REDLOG, along with BIQAA and OSVP, exhibits significantly degraded performance in the $\times 2 \times 4$ scaling factor. This is because these metrics failed to effectively capture scale changes, leading to nearly identical predictions for both $\times 2$ and $\times 4$ scaling factors. The scatter plots of BLIINDS II, TRes, and MANIQA exhibit a positive correlation, but they are not tightly clustered, indicating

TABLE 7. Statistical significance test results on SREB with $\times 2 \times 4$ scaling factor using SRCC.

Method	OSVP	BIQAA	REDLOG	HyperIQA	BLIINDS II	MANIQA	TRes	BRISQUE	SRmetric	KLTSRQA	ReIQA	ARNIQA
OSVP	-	0	0	0	0	0	0	0	0	0	0	0
BIQAA	1	-	0	0	0	0	0	0	0	0	0	0
REDLOG	1	1	-	0	0	0	0	0	0	0	0	0
HyperIQA	1	1	1	-	0	0	0	0	0	0	0	0
BLIINDS II	1	1	1	1	-	0	0	0	0	0	0	0
MANIQA	1	1	1	1	1	-	0	0	0	0	0	0
TRes	1	1	1	1	1	1	-	0	0	0	0	0
BRISQUE	1	1	1	1	1	1	1	-	0	0	0	0
SRmetric	1	1	1	1	1	1	1	1	-	0	0	0
KLTSRQA	1	1	1	1	1	1	1	1	1	-	0	0
ReIQA	1	1	1	1	1	1	1	1	1	1	-	0
ARNIQA	1	1	1	1	1	1	1	1	1	1	1	-

a lower correlation. The HyperIQA exhibited a converged distribution, yet it showed a weak linear relationship standing vertically. Conversely, scatter plots of ReIQA and ARNIQA depict tightly clustered distributions closely aligned along a line with a slope of 1, indicating a strong positive correlation between predicted scores and MOS.

C. STATISTICAL SIGNIFICANCE TEST

To examine whether there are statistically significant differences in performance among the IQA metrics, we conducted statistical significance based on the method proposed in [30]. For each metric, 80% of the data was randomly sampled to predict scores, and the SRCC between the predicted scores and the MOS was calculated. This process was repeated 10,000 times, resulting in 10,000 SRCC for each metric. Subsequently, the Kruskal–Wallis test [52] was applied to assess whether the differences in performance between pairs of metrics were statistically significant. The null hypothesis was defined as follows: the median SRCC of one metric is equal to that of another at a 99% confidence level. Table 7 presents the results of the Kruskal–Wallis test conducted for the $\times 2 \times 4$ scaling factor of the SREB dataset. A value of 1 was assigned if the row metric surpassed the column metric, 0 if it underperformed, and – if there was no significant difference between the two. Metrics with lower performance are placed in the upper rows, and those with higher performance toward the lower rows. The experimental results showed significant performance differences across all metrics, with ARNIQA outperforming all others and achieving the best results. Next in order of performance were ReIQA, KLTSRQA, and SRmetric. These findings are consistent with the results presented in Table 6, clearly demonstrating that ARNIQA and ReIQA, which learn degradation representations while considering scale, perform better than SRmetric and KLTSRQA, both of which are SR-IQA methods.

D. RECEIVER OPERATING CHARACTERISTIC ANALYSIS

In addition to the correlation-based evaluation, we conducted a Receiver Operating Characteristic (ROC) analysis to provide a complementary perspective on metric performance.

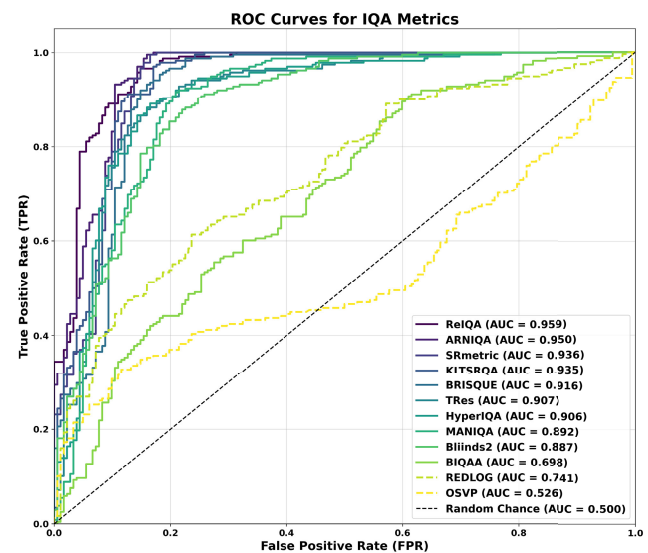


FIGURE 14. ROC curves and AUC values for the 12 tested IQA metrics on our dataset. Solid and dashed lines represent NR and RR metrics, respectively. A curve closer to the top-left corner indicates superior performance in classifying image quality.

This approach assesses the ability of each metric to function as a binary classifier, distinguishing between images of “Good” and “Bad” quality. For this analysis, the ground truth was established by binarizing the MOS; images with $\text{MOS} > 0$ were classified as the “Good” class, while those with $\text{MOS} \leq 0$ were classified as the “Bad” class. The resulting ROC curves and the corresponding Area Under the Curve (AUC) values for all tested metrics are presented in Fig. 14. The analysis reveals that most metrics perform significantly better than random chance (AUC = 0.5). As shown in Fig. 14, ReIQA achieved the highest classification performance with an AUC of 0.959. This was closely followed by ARNIQA, SRmetric, and KLTSRQA, with AUC values of 0.950, 0.936, and 0.935, respectively. This indicates that these top-performing metrics are highly effective at distinguishing between images that subjects perceived as having good versus bad quality. Notably, The performance ranking based on AUC differs slightly from the correlation-based rankings (SRCC, PLCC). This suggests

that some metrics may be stronger at overall rank-ordering, while others excel at separating the two quality classes, thus providing a more multi-faceted understanding of each metric's strengths on our proposed dataset.

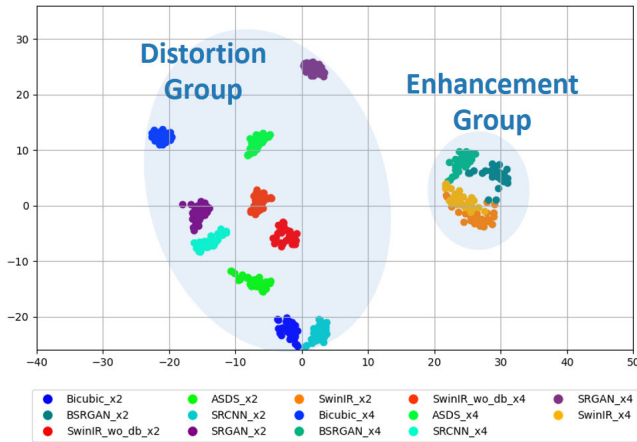


FIGURE 15. t-SNE visualization of ARNIQA features extracted from the SREB dataset.

E. LIMITATIONS AND POTENTIAL OF ARNIQA

To analyze the strengths and limitations of ARNIQA, which demonstrated superior performance on the SREB dataset, we visualized its feature representations using t-distributed Stochastic Neighbor Embedding (t-SNE), as shown in Fig. 15. In this visualization, images processed by the same SR method were assigned the same color. Since ARNIQA employs an encoder trained via contrastive learning to effectively capture quality characteristics under various distortions, a clear clustering was observed between distorted and enhanced SR images. In addition, partial clustering according to SR method was also observed. However, some overlap among the clusters for different SR methods were present, indicating that the separation among SR methods was not fully distinct. The model also exhibited limited ability to distinguish images with different scaling factors. This may be attributed to the encoder being trained solely on diverse distortions, without explicitly learning to distinguish between different SR methods or scaling factors. To address this, future SR IQA models should incorporate images processed with diverse SR methods and scaling factors during contrastive learning, allowing the model to learn and better distinguish these characteristics.

VI. CONCLUSION

This study proposed the SREB dataset to assess the perceptual quality of SR images generated from low-quality broadcast sources. Without downsampling the original content, SR images were created at $\times 2$ and $\times 4$ scales using seven SR methods. Subjective quality assessments revealed that SwinIR achieved the best perceptual quality, and quality decreased with higher scaling factors. Major distortions observed in SR images included blur, noise, and loss of

details. Existing IQA metrics were evaluated on the dataset, and ARNIQA showed the highest correlation with human scores by effectively modeling distortion types. However, most metrics struggled with the combination of different scaling factors. These experimental results confirm that the SREB dataset is sufficiently robust to draw these meaningful conclusions about metric performance.

We acknowledge our deliberate focus on single-frame SR. This approach allows the SREB dataset to serve as a controlled, foundational baseline for assessing spatial quality when SR is applied to challenging, low-quality legacy sources. Establishing such a benchmark is essential, as it enables focused research on how various SR methods handle realistic spatial artifacts. This, in turn, provides a necessary foundation before tackling the combined spatio-temporal complexities of VSR. Therefore, the SREB dataset is presented not only as a tool for developing improved IQA metrics that consider scaling effects and realistic distortions found in low-quality content, but also as a cornerstone that supports the expansion of research into comprehensive video quality assessment.

ACKNOWLEDGMENT

(Yongrok Kim and Junha Shin contributed equally to this work.)

REFERENCES

- [1] Y. Yoon, H.-G. Jeon, D. Yoo, J.-Y. Lee, and I. S. Kweon, "Learning a deep convolutional network for light-field image super-resolution," in *Proc. IEEE Int. Conf. Comput. Vis. Workshop (ICCVW)*, Dec. 2015, pp. 57–65.
- [2] C. Dong, C. C. Loy, and X. Tang, "Accelerating the super-resolution convolutional neural network," in *Proc. Eur. Conf. Comput. Vis.*, 2016, pp. 391–407.
- [3] J. Kim, J. K. Lee, and K. M. Lee, "Accurate image super-resolution using very deep convolutional networks," in *Proc. IEEE Conf. Comput. Vis. Pattern Recognit.*, Jun. 2016, pp. 1646–1654.
- [4] C. Ledig, L. Theis, F. Huszár, J. Caballero, A. Cunningham, A. Acosta, A. Aitken, A. Tejani, J. Totz, Z. Wang, and W. Shi, "Photo-realistic single image super-resolution using a generative adversarial network," in *Proc. IEEE Conf. Comput. Vis. Pattern Recognit. (CVPR)*, Jul. 2017, pp. 105–114.
- [5] K. Zhang, J. Liang, L. V. Gool, and R. Timofte, "Designing a practical degradation model for deep blind image super-resolution," in *Proc. IEEE Int. Conf. Comput. Vis.*, Oct. 2021, pp. 4791–4800.
- [6] J. Liang, J. Cao, G. Sun, K. Zhang, L. V. Gool, and R. Timofte, "SwinIR: Image restoration using Swin transformer," in *Proc. IEEE Int. Conf. Comput. Vis.*, Oct. 2021, pp. 1833–1844.
- [7] G. Cho and Y. S. Choi, "Image super-resolution with unified-window attention," *IEEE Access*, vol. 12, pp. 30852–30866, 2024.
- [8] Z. Wang, A. C. Bovik, H. R. Sheikh, and E. P. Simoncelli, "Image quality assessment: From error visibility to structural similarity," *IEEE Trans. Image Process.*, vol. 13, no. 4, pp. 600–612, Apr. 2004.
- [9] R. Zhang, P. Isola, A. A. Efros, E. Shechtman, and O. Wang, "The unreasonable effectiveness of deep features as a perceptual metric," in *Proc. IEEE/CVF Conf. Comput. Vis. Pattern Recognit.*, Jun. 2018, pp. 586–595.
- [10] J. Wu, W. Lin, G. Shi, L. Li, and Y. Fang, "Orientation selectivity based visual pattern for reduced-reference image quality assessment," *Inf. Sci.*, vol. 351, pp. 18–29, Jul. 2016.
- [11] S. Golestaneh and L. J. Karam, "Reduced-reference quality assessment based on the entropy of DWT coefficients of locally weighted gradient magnitudes," *IEEE Trans. Image Process.*, vol. 25, no. 11, pp. 5293–5303, Nov. 2016.

[12] L. Tang, K. Sun, L. Liu, G. Wang, and Y. Liu, “A reduced-reference quality assessment metric for super-resolution reconstructed images with information gain and texture similarity,” *Signal Process., Image Commun.*, vol. 79, pp. 32–39, Nov. 2019.

[13] A. Mittal, A. K. Moorthy, and A. C. Bovik, “No-reference image quality assessment in the spatial domain,” *IEEE Trans. Image Process.*, vol. 21, no. 12, pp. 4695–4708, Dec. 2012.

[14] A. Mittal, R. Soundararajan, and A. C. Bovik, “Making a ‘completely blind’ image quality analyzer,” *IEEE Signal Process. Lett.*, vol. 20, no. 3, pp. 209–212, 2013.

[15] A. K. Moorthy and A. C. Bovik, “Blind image quality assessment: From natural scene statistics to perceptual quality,” *IEEE Trans. Image Process.*, vol. 20, no. 12, pp. 3350–3364, Dec. 2011.

[16] F. Zhou, R. Yao, B. Liu, and G. Qiu, “Visual quality assessment for super-resolved images: Database and method,” *IEEE Trans. Image Process.*, vol. 28, no. 7, pp. 3528–3541, Jul. 2019.

[17] Q. Jiang, Z. Liu, K. Gu, F. Shao, X. Zhang, H. Liu, and W. Lin, “Single image super-resolution quality assessment: A real-world dataset, subjective studies, and an objective metric,” *IEEE Trans. Image Process.*, vol. 31, pp. 2279–2294, 2022.

[18] S.-j. Shi, J. Xu, L. Lu, Z. Li, and K. Hu, “Self-supervised ControlNet with spatio-temporal mamba for real-world video super-resolution,” in *Proc. IEEE/CVF Conf. Comput. Vis. Pattern Recognit. (CVPR)*, Jun. 2025, pp. 7385–7395.

[19] E. Kim, H. Kim, K. H. Jin, and J. Yoo, “BF-STVSR: B-splines and Fourier—Best friends for high fidelity spatial-temporal video super-resolution,” in *Proc. IEEE/CVF Conf. Comput. Vis. Pattern Recognit. (CVPR)*, Jun. 2025, pp. 28009–28018.

[20] Y. Xu, T. Park, R. Zhang, Y. Zhou, E. Shechtman, F. Liu, J. Huang, and D. Liu, “VideoGigaGAN: Towards detail-rich video super-resolution,” in *Proc. IEEE/CVF Conf. Comput. Vis. Pattern Recognit. (CVPR)*, Jun. 2024, pp. 2139–2149.

[21] H. R. Sheikh, M. F. Sabir, and A. C. Bovik, “A statistical evaluation of recent full reference image quality assessment algorithms,” *IEEE Trans. Image Process.*, vol. 15, no. 11, pp. 3440–3451, Nov. 2006.

[22] K. Gu, M. Liu, G. Zhai, X. Yang, and W. Zhang, “Quality assessment considering viewing distance and image resolution,” *IEEE Trans. Broadcast.*, vol. 61, no. 3, pp. 520–531, Sep. 2015.

[23] G. Yue, H. Wu, W. Yan, T. Zhou, H. Liu, and W. Zhou, “Subjective and objective quality assessment of multi-attribute retouched face images,” *IEEE Trans. Broadcast.*, vol. 70, no. 2, pp. 570–583, Jun. 2024.

[24] C. Y. Yang, C. Ma, and M.-H. Yang, “Single-image super-resolution: A benchmark,” in *Proc. Eur. Conf. Comput. Vis.*, 2014, pp. 372–386.

[25] H. Yeganeh, M. Rostami, and Z. Wang, “Objective quality assessment of interpolated natural images,” *IEEE Trans. Image Process.*, vol. 24, no. 11, pp. 4651–4663, Nov. 2015.

[26] C. Ma, C.-Y. Yang, X. Yang, and M.-H. Yang, “Learning a no-reference quality metric for single-image super-resolution,” *Comput. Vis. Image Understand.*, vol. 158, pp. 1–16, May 2017.

[27] G. Shi, W. Wan, J. Wu, X. Xie, W. Dong, and H. R. Wu, “SISRSet: Single image super-resolution subjective evaluation test and objective quality assessment,” *Neurocomputing*, vol. 360, pp. 37–51, Sep. 2019.

[28] T. Köhler, M. Bätz, F. Naderi, A. Kaup, A. Maier, and C. Riess, “Toward bridging the simulated-to-real gap: Benchmarking super-resolution on real data,” *IEEE Trans. Pattern Anal. Mach. Intell.*, vol. 42, no. 11, pp. 2944–2959, Nov. 2020.

[29] O. Wiedemann, V. Hosu, S. Su, and D. Saupe, “Konx: Cross-resolution image quality assessment,” *Qual. User Exper.*, vol. 8, no. 1, p. 8, Dec. 2023.

[30] J. Beron, H. D. Benitez-Restrepo, and A. C. Bovik, “Blind image quality assessment for super resolution via optimal feature selection,” *IEEE Access*, vol. 8, pp. 143201–143218, 2020.

[31] W. Sun, F. Zhou, and Q. Liao, “MDID: A multiply distorted image database for image quality assessment,” *Pattern Recognit.*, vol. 61, pp. 153–168, Jan. 2017.

[32] A. Balakhnin. (2009). *Yadif*. [Online]. Available: <https://avisynth.org.ru/yadif/yadif.html>

[33] *Subjective Video Quality Assessment Methods for Multimedia Applications*, document ITU-T Rec P.910, 2008.

[34] D. Hasler and S. E. Suesstrunk, “Measuring colorfulness in natural images,” *Proc. SPIE*, vol. 5007, pp. 87–95, Jun. 2003.

[35] W. Lai, J. Huang, N. Ahuja, and M.-H. Yang, “Deep Laplacian pyramid networks for fast and accurate super-resolution,” in *Proc. IEEE Conf. Comput. Vis. Pattern Recognit.*, Jul. 2017, pp. 5835–5843.

[36] W. Shi, F. Jiang, and D. Zhao, “Single image super-resolution with dilated convolution based multi-scale information learning inception module,” in *Proc. IEEE Int. Conf. Image Process. (ICIP)*, Sep. 2017, pp. 977–981.

[37] K. Zhang, W. Zuo, and L. Zhang, “Learning a single convolutional super-resolution network for multiple degradations,” in *Proc. IEEE/CVF Conf. Comput. Vis. Pattern Recognit.*, Jun. 2018, pp. 3262–3271.

[38] N. Ahn, B. Kang, and K.-A. Sohn, “Fast, accurate, and lightweight super-resolution with cascading residual network,” in *Proc. Eur. Conf. Comput. Vis. (ECCV)*, 2018, pp. 256–272.

[39] Z. Hui, X. Gao, Y. Yang, and X. Wang, “Lightweight image super-resolution with information multi-distillation network,” in *Proc. 27th ACM Int. Conf. Multimedia*, Oct. 2019, pp. 2024–2032.

[40] B. Lim, S. Son, H. Kim, S. Nah, and K. M. Lee, “Enhanced deep residual networks for single image super-resolution,” in *Proc. IEEE Conf. Comput. Vis. Pattern Recognit. Workshops (CVPRW)*, Jul. 2017, pp. 1132–1140.

[41] W. Dong, L. Zhang, G. Shi, and X. Wu, “Image deblurring and super-resolution by adaptive sparse domain selection and adaptive regularization,” *IEEE Trans. Image Process.*, vol. 20, no. 7, pp. 1838–1857, Jul. 2011.

[42] *Methodologies for the Subjective Assessment of the Quality of Television Images*, document ITU-R Rec. BT.500, 2019.

[43] R. A. Bradley and M. E. Terry, “Rank analysis of incomplete block designs: I. The method of paired comparisons,” *Biometrika*, vol. 39, nos. 3–4, pp. 324–345, Dec. 1952.

[44] F. Wilcoxon, *Individual Comparisons by Ranking Methods*. Cham, Switzerland: Springer, 1992, pp. 196–202.

[45] S. Gabarda and G. Cristóbal, “Blind image quality assessment through anisotropy,” *J. Opt. Soc. Amer. A, Opt. Image Sci.*, vol. 24, no. 12, pp. B42–B51, 2007.

[46] M. A. Saad, A. C. Bovik, and C. Charrier, “Blind image quality assessment: A natural scene statistics approach in the DCT domain,” *IEEE Trans. Image Process.*, vol. 21, no. 8, pp. 3339–3352, Aug. 2012.

[47] S. Su, Q. Yan, Y. Zhu, C. Zhang, X. Ge, J. Sun, and Y. Zhang, “Blindly assess image quality in the wild guided by a self-adaptive hyper network,” in *Proc. IEEE/CVF Conf. Comput. Vis. Pattern Recognit. (CVPR)*, Jun. 2020, pp. 3664–3673.

[48] S. A. Golestaneh, S. Dadsetan, and K. M. Kitani, “No-reference image quality assessment via transformers, relative ranking, and self-consistency,” in *Proc. IEEE/CVF Winter Conf. Appl. Comput. Vis. (WACV)*, Jan. 2022, pp. 3989–3999.

[49] S. Yang, T. Wu, S. Shi, S. Lao, Y. Gong, M. Cao, J. Wang, and Y. Yang, “MANIQA: Multi-dimension attention network for no-reference image quality assessment,” in *Proc. IEEE/CVF Conf. Comput. Vis. Pattern Recognit. Workshops (CVPRW)*, Jun. 2022, pp. 1190–1199.

[50] A. Saha, S. Mishra, and A. C. Bovik, “Re-IQA: Unsupervised learning for image quality assessment in the wild,” in *Proc. IEEE/CVF Conf. Comput. Vis. Pattern Recognit. (CVPR)*, Jun. 2023, pp. 5846–5855.

[51] L. Agnolucci, L. Galteri, M. Bertini, and A. Del Bimbo, “ARNIQA: Learning distortion manifold for image quality assessment,” in *Proc. IEEE/CVF Winter Conf. Appl. Comput. Vis. (WACV)*, Jan. 2024, pp. 188–197.

[52] W. H. Kruskal and W. A. Wallis, “Use of ranks in one-criterion variance analysis,” *J. Amer. Stat. Assoc.*, vol. 47, no. 260, pp. 583–621, Dec. 1952.



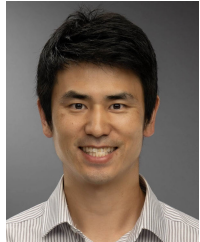
YONGROK KIM received the B.S. degree from the School of Electrical Engineering, Hanyang University, ERICA Campus, Ansan, South Korea, in 2020, where he is currently pursuing the integrated M.S. and Ph.D. degree with the Department of Electrical and Electronic Engineering. His research interests include visual quality assessment and deep learning-based image restoration.



JUNHA SHIN received the B.S. degree from the School of Electrical Engineering, Hanyang University, ERICA Campus, Ansan, South Korea, in 2023, where he is currently pursuing the integrated M.S. and Ph.D. degree with the Department of Electrical and Electronic Engineering. His research interests include perceptual visual quality assessment, deep learning-based image quality assessment, and generative model.



HYUNSUK KO (Member, IEEE) received the B.S. and M.S. degrees from the Department of Electrical Engineering, Yonsei University, Seoul, South Korea, in 2006 and 2009, respectively, and the Ph.D. degree from the Department of Electrical Engineering, University of Southern California, Los Angeles, CA, USA, in 2015. From 2015 to 2020, he was a Senior Researcher with the Electronics and Telecommunications Research Institute. He is currently an Associate Professor with the School of Electrical Engineering, Hanyang University, ERICA Campus, Ansan, South Korea. His research interests include video coding, perceptual visual quality assessment, computer vision, and deep learning-based multimedia signal processing.



JUHYUN LEE received the Bachelor of Science (B.S.) degree in biomedical engineering from The University of Utah, in 2010, the master's degree from the University of Southern California (USC), and the Ph.D. degree in bioengineering from the University of California, Los Angeles (UCLA). He currently holds the position of an Associate Professor with the Department of Bioengineering, The University of Texas at Arlington (UTA). Following his academic training, he briefly transitioned to the industry, working as a Biomedical Engineer with Edward Lifesciences. After coming back to academia, he has been dedicated to advancing the field of high-resolution microscopy for *in vivo* dynamic imaging techniques.